When a Single Chip becomes the RFID Reader: An Ultra-low-cost $60\,\mathrm{GHz}$ Reader and mmID System for Ultra-accurate 2D Microlocalization

Charles A. Lynch III*, Ajibayo O. Adeyeye*, J. G.D. Hester†, Manos M. Tentzeris*
*School of Electrical and Computer Engineering
Georgia Institute of Technology
Atlanta, GA, USA
clynch19@gatech.edu
†Atheraxon
Atlanta, GA, USA
jimmy.hester@atheraxon.com

2021 IEEE International Conference on RFID (RFID) | 978-1-6654-4090-5/20/$31.00 ©2021 IEEE | DOI: 10.1109/RFID52461.2021.9444319

Abstract*—In this work, a mmID tag and reader system operating in the $60\,\mathrm{GHz}$ ISM band is proposed. The sticker-form factor-mmID-tag has a total footprint of only $3.5\,\mathrm{cm}$ by $1.5\,\mathrm{cm}$ and is fabricated utilizing ultra-low cost inkjet-printed PCB technology and components. For the first time, a low-cost and ultra-compact antenna-on-package radar module is utilized for the reader system, to provide accurate microlocalization of the mmID tags in 2D space. One proof-of-concept tag was successfully localized at various steps of $5\,\mathrm{cm}$ from a range of $10\,\mathrm{cm}$ to $50\,\mathrm{cm}$ with a maximum deviation of $4.46\,\mathrm{cm}$. The reader system also demonstrated the ability to detect the Angle-of-Arrival at a range of $15\,\mathrm{cm}$ in angular steps of $20\,^{\circ}$ providing an angular coverage of $\pm 40\,^{\circ}$. Lastly, the total power consumption of the mmID tag was measured at a mere $1.43\,\mathrm{mW}$, allowing for long term usage of the tag in autonomous settings. This work potentially introduces a paradigm shift in the application of backscatter systems by introducing an affordable mmID-enabled real-time-microlocalization solution compatible with inconspicuous ubiquitous and wearable implementations.

***Index Terms*—mmWave, mmID, Localization, IoT**

I. Introduction

In recent years, the employment of Radio Frequency Identification (RFID) technology in Internet of Things (IoT) applications has increased significantly. Through reduced costs, simplification of system components, and ultra-low power consumptions, these RFID tags have been utilized for wireless communications, sensing, and localization in a growing number of IoT applications. However, these systems mostly utilize RFID tags operating in the Ultra High Frequency (UHF) band. Due to their inherently limited bandwidth available and to their impractically-large size of antenna arrays at this frequency of operation, the tags are generally limited in localization accuracy and require large system components for both reader and RFID front-ends.

In order to achieve higher fidelity, ranging accuracy and more compact reader/tag designs, Millimeter-Wave Identification (mmID) devices are one potential solution. In [1] and [2] feasibility and demonstration of utilizing mmID technology as a replacement for UHF RFID technology was presented. Additionally, [1] proposed applications based on high data rate communication and transponder communication with an automotive radar. These high data rates are made possible through the much broader available bandwidth at mmWave. In [3], the authors demonstrated high data rate capabilities of mmID through backscattering with reported data rates of on the order of gigabits per second. The high data rate capabilities of mmID technology are specifically applicable for smart home devices, that can communicate with each other to provide a home network for more efficient usage, or other human interfaces that are dependent on the precise localization of objects. With respect to the reader systems at these mm-wave frequencies, a natural choice would be Frequency-Modulated Continuous Wave (FMCW) radar modules, which are becoming commodities and, therefore, remarkably mature and accessible. Thus, an FMCW radar system provides a cheap reader solution that can simultaneously locate in 2D and identify tags in its field of view. The authors in [4] displayed the usage both a miniaturized MMID tag with an FMCW reader system for localization up to a total range of $0.3\,\mathrm{m}$, with a standard deviation of $1.02\,\mathrm{cm}$ in the range measurement. This system was operating in the $24\,\mathrm{GHz}$ Industrial, Scientific, and Medical (ISM) band and, therefore, has a limit in maximum effective isotropic radiated power (EIRP) and a bandwidth of $12\,\mathrm{dBm}$ and $250\,\mathrm{MHz}$, respectively. These limitations in the available spectrum heavily restrict the range resolution and accuracy of this system. In addition, $24\,\mathrm{GHz}$ FMCW radar modules remain too large for many (including wearable) applications. Therefore, higher-operating-frequency systems are called for. In [5], the authors present an active $34.5\,\mathrm{GHz}$ MMID system used for localization, but despite the fact that the system doubled the available bandwidth compared to $24\,\mathrm{G}$ ISM band, it required a bulky reader, making the reader system unappealing for the low-cost applications considered in our effort. Additionally, this frequency band is not an allocated ISM band effectively limiting its widespreade use.

Thus, with the recent updated restrictions of the $60\,\mathrm{GHz}$

978-1-6654-4090-5/21/$31.00 ©2021 IEEE

978-1-6654-4090-5/21/$31.00 ©2021 IEEE

ISM band, its use for mmID systems becomes extremely appealing. Indeed, it allows for low cost and miniaturized system components, more available bandwidth and, consequently, increased range resolutions. For instance, in [6] the authors proposed a millimeter wave radar for ubiquitous gesture recognition with the radar system operating on a single chip. Such approaches can be greatly enhanced through the use of mmID tags, thereby simultaneously introducing capabilities yet unavailable to current backscatter systems. The authors in [7] reported the design, ranging, and localization of a 61 GHz tag with an FMCW radar, but the entire system was, once again, bulky and required a high-gain lens to achieve the reported ranges and accuracy. In an effort to fully utilize the advantages endowed by the use of the 60 GHz ISM band, the authors in this work present an ultra low-cost, ultra-compact mmWave mmID system for the purpose of 2D spatial identification and tag localization. A system level diagram of the short-range localization system is displayed in Figure 1. The remainder of

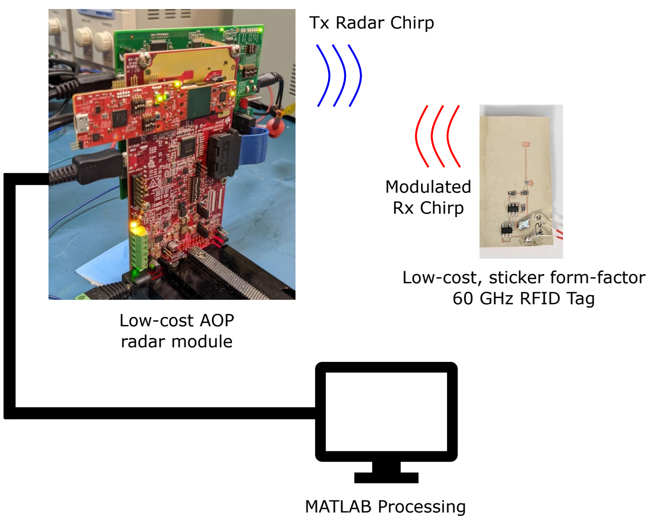

Fig. 1. mmWave identification and localization system level schematic of the proposed compact, low cost, short range localization system.

this paper is organized as follows: In Section II, the designs of the front-end and baseband circuitry are described. In Section III, the FMCW radar interrogation system and post-processing scheme used to estimate the position of the tag in 2D space is described. In Section IV, the results from ranging and Angle-of-Arrival (AoA) measurements are presented. Finally, in Section V, the authors conclude the work.

II. Low-Cost mmWave Tag Design

The mmID tag is comprised of two main components: the RF Front-end—which enables backscattering of the transmitted radar chirp signal back to the reader—and the baseband circuitry, to control the modulation. The tag itself has a metal-backed (and, therefore, support-agnostic) sticker-like form-factor, which is appealing for many IoT applications. An image of the complete tag can be viewed in Figure 2. The total footprint of the low cost tag currently is $3.5\,\mathrm{cm} \times 1.5\,\mathrm{cm}$, which could be reduced by more than 80% through the use of dedicated ICs and through tighter packing of its layout.

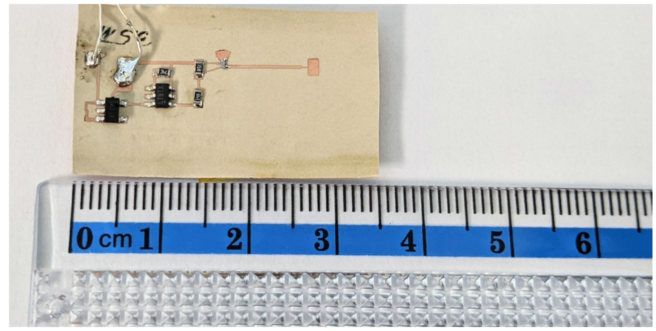

Fig. 2. Planar, printed, low-cost mmWave tag.

A. Front-end Design

The patch antenna was designed to operate over the entire 60 GHz to 64 GHz band covered by the FMCW radar/reader. The substrate selected was on Rogers 3003 ($\epsilon = 3.0, tan(\delta) = 0.0010$) with a thickness of $0.127\,\mathrm{m}$. This substrate is ideal for mmWave designs as it provides a low-cost and low-loss compromise. The patch antenna was designed in CST Microwave Studio and a quarter-wave length matching section was utilized to match the input impedance of the antenna to a $50\,\Omega$ transmission line. The antenna design is critical in a backscattering link, as the losses in the antenna are doubled because of the two way propagation of the backscattered signal. The return loss of the antenna, shown in Figure 3, shows that the antenna is best matched at $61.8\,\mathrm{GHz}$ with a $-10\,\mathrm{dB}$ of matching throughout the entire band of interest. Additionally, the estimated $3\,\mathrm{dB}$ beamwidth of the patch antenna was simulated to be $\pm 40\,^\circ$ from boresight of antenna. Thus, the proposed patch antenna would provide good performance of backscattering the incoming radar chirp back to the interrogator for both range and AoA measurements within an $80\,^\circ$ beamwidth with respect to the reader.

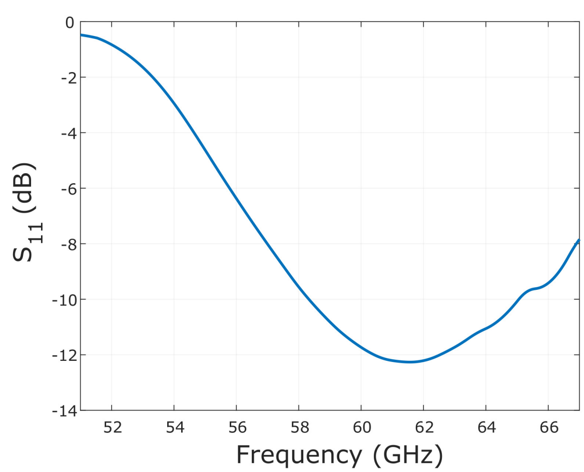

Fig. 3. Measured return loss for the patch antenna design.

The second component of the front-end is the switchable load, which modulate the incoming radar chirp to isolate the backscattered signal from the reader's self-interference and encode information (such as identity, for instance). The modulation for this work was amplitude-based modulation, which was implemented by utilizing a low-cost MADS-001317-1500 schottky diode from Macom. The diode was designed to present two loads states to the incoming radar chirp with bias voltages of either $0\,\mathrm{V}$ or $0.85\,\mathrm{V}$. In Figure 4, one can view a magnitude modulation-depth of $6\,\mathrm{dB}$ at center of the band, enabling an acceptable modulation of the received signal. The measured modulation factor M in dB calculated through the expression

$$M = \frac{1}{4}|\Gamma_{0.85\,\mathrm{V}} - \Gamma_{0\,\mathrm{V}}| \tag{1}$$

, where $\Gamma_{0.85\,\mathrm{V}}$ and $\Gamma_{0\,\mathrm{V}}$ are the reflection coefficients of the load of the $0.85\,\mathrm{V}$ and $0\,\mathrm{V}$ bias states, respectively. The modulation factor was calculated to be $-13\,\mathrm{dB}$. An annotated circuit layout of the integrated front-end designed is shown in Figure 5.

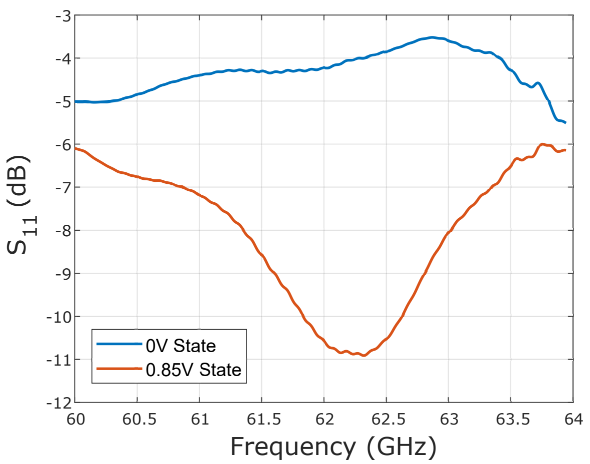

Fig. 4. Measured one-port parameter of switch for the two modulation states.

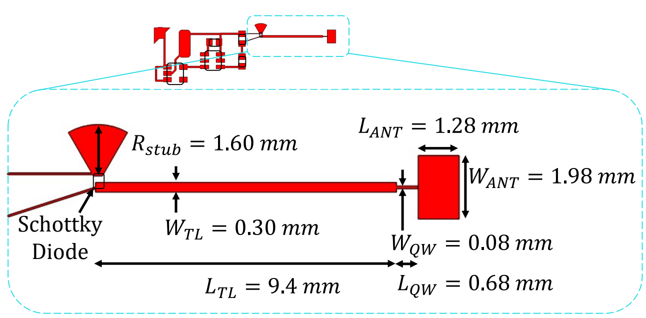

Fig. 5. Layout of the low-cost integrated front-end.

B. Baseband Circuit Design

The baseband circuitry is composed of an ultra-low-power linear voltage regulator XC6504A301MR-G, a resistance-based voltage controlled oscillator (VCO) LTC6907, and two bias resistors that act as a voltage divider to provide the appropriate bias voltage to the schottky diode. The voltage regulator provides a stable output voltage that is fed into the VCO. The regulator and VCO are essential to the ranging extraction. As explained in Section III, the ranging information extracted by the FMCW systems is linearly-dependent on frequency-peaks measured in the baseband spectrum. Therefore, with unstable voltages and oscillation frequencies, jitter could greatly spoil the ranging information. Additionally, the resistance-based VCO allows simple Frequency Division Multiplexing (FDM), where each tag's modulation frequency can be used as a unique ID, thereby enabling the simultaneousl localization of mulitple tags in the field-of-view of the radar. The output of the VCO is a $3.1\,\mathrm{V}$ square wave at the set frequency and, therefore, a voltage divider consisting of a $1.36\,\mathrm{k\Omega}$ and a $3.6\,\mathrm{k\Omega}$ resistor provided the necessary voltage divider to appropriately bias the schottky diode. The set resistor was set to a value of $52.3\,\mathrm{k\Omega}$ resulting in a modulation frequency of $3.824\,\mathrm{MHz}$. The current draw for the baseband circuitry with this modulation frequency, recorded with the 6485 Keithley PicoAmmeter was $156\,\mu\mathrm{A}$. Therefore, this simple, low cost tag design allows the creation of a sub-carrier that uniquely identifies and can be used to accurately localize the tag with an FMCW radar as the reader. An annotated layout of the baseband circuit is shown in Figure 6.

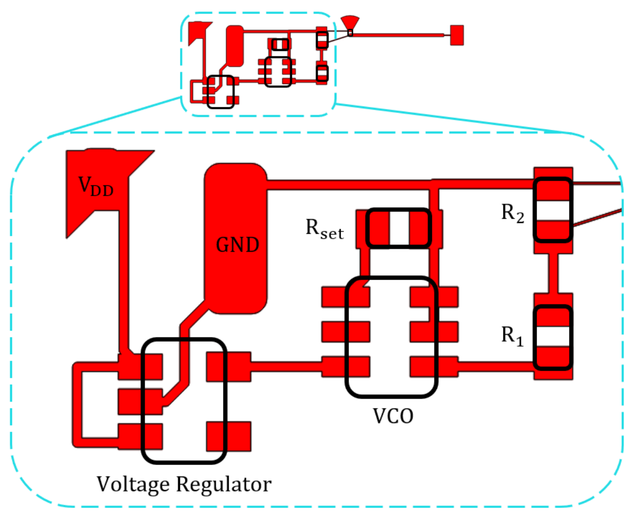

Fig. 6. Layout of low-cost baseband circuitry with annotated components.

C. Fabrication of Fully Integrated mmID Tag

Once both the front-end and baseband circuit designs were finalized. The fully integrated mmID tag was fabricated utilizing an inkjet masking procedure with Microchem SU-8 and the Dimatix DMP-2831 printer, with a printing resolution of $20\,\mu\mathrm{m}$. Once the mask was printed on one side of the copper clad Rogers 3003 substrate, the SU-8 was cured and then etched in a ferrochloride bath. Utilizing a 6485 Keithley PicoAmmeter, the average current consumption of the entire tag was estimated to be $460\,\mu\mathrm{A}$ resulting in a total power consumption of $1.43\,\mathrm{W}$ with a $3.1\,\mathrm{V}$ supply. In Table I, the power consumption of each component of the mmID is detailed.

TABLE I
BREAKDOWN OF POWER CONSUMPTION OF LOW-COST MMID TAG.

Circuit	**Power Consumption** (mW)
Front-end	0.95 mW
Baseband	0.48 mW
Fully Integrated Tag	1.43 mW

This power consumption is lower than that of commercial active IoT transceivers and, thus, provides the ability for relatively long-term daily usage of this device for such applications.

III. PROPOSED READER AND SIGNAL PROCESSING FRAMEWORK

The radar module utilized in proposed reader system is the IWR6843AOP EVM module from Texas Instruments (TI). This module consists of three transmit and four receive channels with on-package patch antennas with 5 dBi of gain, a maximum transmitted power of 10 dBm, a wide field of view of $\pm 120^\circ$ in azimuth and elevation, and a compact Antenna on Package form factor making this module a ultra-low cost, ultra-compact reader for IoT mmID-enabled localization systems. The maximum reading range of the proposed low-cost mmID micro-localization system can be estimated through a link budget analysis and referencing the received power level to the reader sensitivity. The sample rate utilized for the thermal noise level estimation was calculated through dividing the baseband sampling rate by the length of the fast-Fourier transform utilized to estimate the frequency domain of the received spectrum. An estimation of the theoretical maximum reading range of the current and ideal future system is detailed in Table II

TABLE II
LINK BUDGET ANALYSIS OF CURRENT AND IDEAL FUTURE SYSTEM.

Parameter	**Current System**	**Ideal Future System**
P_{Tx}	10 dBm	14 dBm
G_{Tx}	5 dBi	6 dBi
G_{Rx}	5 dBi	20 dBi
G_{Tag}	4 dBi	15 dBi
M	-13 dB	-6 dB
S @ 6.56 kHz Sampling Rate	-102.82 dB	-124.83 dB
Max Range @ 6.56 kHz Sampling Rate	0.90 m	48.17 m

, where P_{Tx}, G_{Tx}, G_{Rx}, G_{tag}, M, and S are the transmitted power, antenna gain of the transmitter, antenna gain of the receiver, antenna gain of the mmID tag, modulation factor of the mmID tag, and reader sensitivity, respectively. Through establishing a minimum signal-to-noise ratio of 3 dB, the estimated maximum range of the current system is approximately 90 cm making the system suitable for short-range localization applications. However, an ideal future system with improvement to the mmID modulation factor, utilization of a cross-polarized antenna array for the mmID, and increased sensitivity of a cross-polarized reader architecture, displays a theoretical maximum range 48.17 m, enabling medium to long range IoT localization applications. This Multiple Input, Multiple Output (MIMO) FMCW antenna-enabled module current retails for less than 20\$, more than an order of magnitude cheaper than typical UHF mmID readers and, with its 15 mm x 15 mm dimensions (antennas included), more than 100x more compact. The radar module is displayed in Figure 7. In

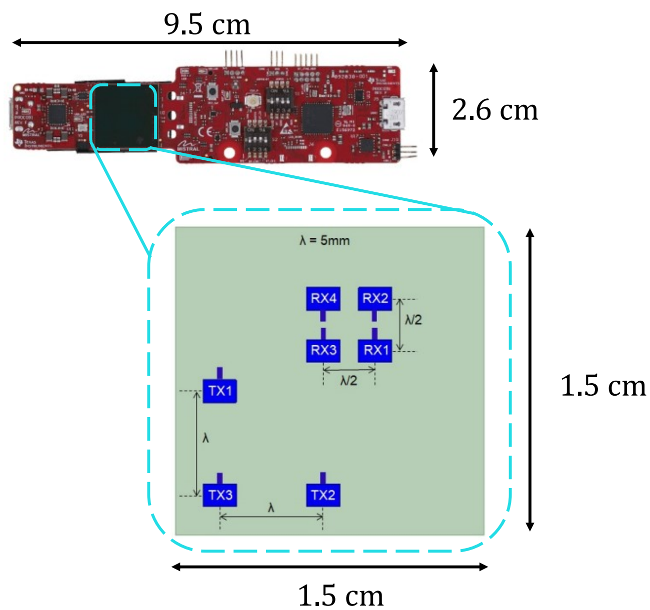

Fig. 7. IWR6843AOP EVM module utilized in mmID Reader System.

order to extract the raw Analog to Digital Converter (ADC) values of the from the radar the MMWAVEICBOOST and the DCA1000EVM boards from TI were utilized, subsequent to which the baseband signal channels were processed in MATLAB.

A. Estimation of tag ranges

The transmitted Linear Frequency Modulated (LFM) time domain signal for $t = [0, T_c]$—where T_c is the chirp duration time for the proposed reader—can be expressed as

$$s_{Tx}(t) = A * exp\left(j2\pi\left(f_c t + \frac{B}{T_c}t^2 + \phi_o\right)\right) \quad (2)$$

, where A, f_c , B, and ϕ_o are the amplitude, carrier frequency, sweeping bandwidth, and initial phase of transmitted waveform, respectively. For a backscattering target with a modulation frequency of f_{mod} the received waveform can be expressed as $s_{Rx} = s_{Tx}(t - \tau) * exp(j2\pi f_{mod})$, where τ is the round trip time of radiation to travel to the backscattering target and back to the reader which can be expressed as

$$\tau = \frac{2R}{c} \tag{3}$$

, where R and c are the range of the backscattering target and the phase celerity of the electromagnetic wave, respectively.

After mixing with s_{Tx} and applying a low-pass filter, the resulting baseband signal can be expressed as

$$\begin{aligned} s_{Rx}(t) = \alpha A exp\Bigg(j2\pi \Bigg(\frac{B}{T_c}\tau \pm f_{mod} \\ + \frac{2R}{\lambda} + \phi_{tag} + \phi_o \Bigg)\Bigg) \end{aligned} \tag{4}$$

, where α and ϕ_{tag} are the attenuation of the signal from round trip travel back to the reader, and the random starting phase of the tag modulation signal,respectively. A fast-Fourier transform (FFT) along a single chirp is taken to extract f_{beat}, the beat frequency, which encapsulates the ranging information and is expressed as

$$f_{beat} = \frac{B}{T_c}\tau. \tag{5}$$

For a receiver with In-phase and Quadrature channels, the resultant beat frequency of the backscattering target will have both positive and negative spectral components at the frequencies $f_{mod} + f_{beat}$ and $f_{beat} - f_{mod}$. Therefore, in order to obtain the desired R or range of the tag, one can simply use the expression

$$R = \frac{f_{mod} + f_{beat} + (f_{beat} - f_{mod})}{2} * \frac{cT_c}{B} \tag{6}$$

to estimate the range of the tag. In order to extend the range of the tag, first a range-FFT along each chirp in the frame was conducted and the magnitude spectrum of each range-FFT result was averaged. The range was then estimated using Equation 6. A visualization of the range extraction signal processing framework is displayed in Figure 8

B. Estimation of tag AoA

Angle-of-Arrival information in any radar system is dependent on the physical placement of the transmitting and receiving antennas and requires at least two channels. In the simple case of one transmitting and two receiving antennas, the AoA estimate is based on the instantaneous difference in phase of a target across the two receiving channels. This estimate can be expressed as

$$\theta = sin^{-1}\left(\frac{\lambda\omega}{2\pi d}\right), \tag{7}$$

where θ, λ, ω, and d are the AoA estimate in degrees, free-space wavelength, phase difference across two channels, and spacing of the two receiving antennas, respectively. The four receiver antennas on the IWR6843AOPEVM have an element

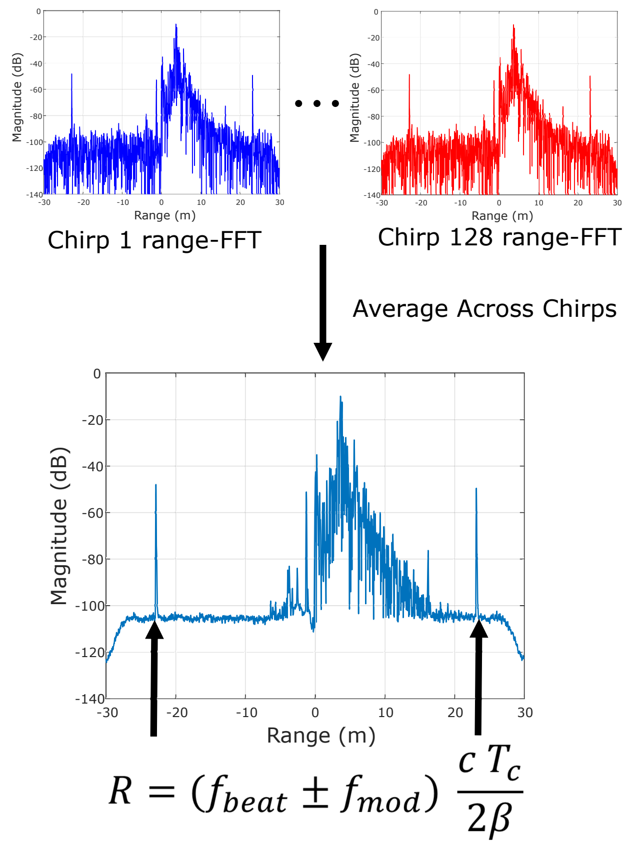

Fig. 8. Signal processing framework for range estimate of mmID tag.

spacing of $d = \frac{\lambda}{2}$ resulting in a $\pm 90\,^{\circ}$ of AoA discrimination. In order to extract the AoA estimate, after taking the range-FFT and identifying the modulated beat frequencies, an angle-FFT was conducted on the peaks of the positive modulated beat frequency across two receive channels. This process was applied across each chirp in a single frame and the magnitude spectrum of each chirp was averaged. The peak value of this averaged magnitude spectrum of the angle-FFT was then selected as the estimated angle. A visualization of the signal processing framework for the AoA estimate can be viewed in Figure 9.

IV. BENCHMARKING OF THE LOCALIZATION SYSTEM

Range measurements with the mmID tag, placed on a millimeter accurate track directly boresight to the radar module, were conducted. The true measurements distances were measured utilizing a Fluke 419D laser distance measuring device. The chirp parameters of the reader for these measurements can be viewed in Table III. Chirp parameters play a critical role in the governing the maximum unambiguous range and the maximum resolution of the range measurement. For the case of these measurements, the maximum Intermediate Frequency (IF) that can be measured was $5\,\text{MHz}$ which corresponds to a maximum unambiguous range of $29.997\,\text{m}$. The range resolution, based on the sweeping bandwidth is $3.944\,\text{cm}$. The number of complex-valued samples taken for each chirp were

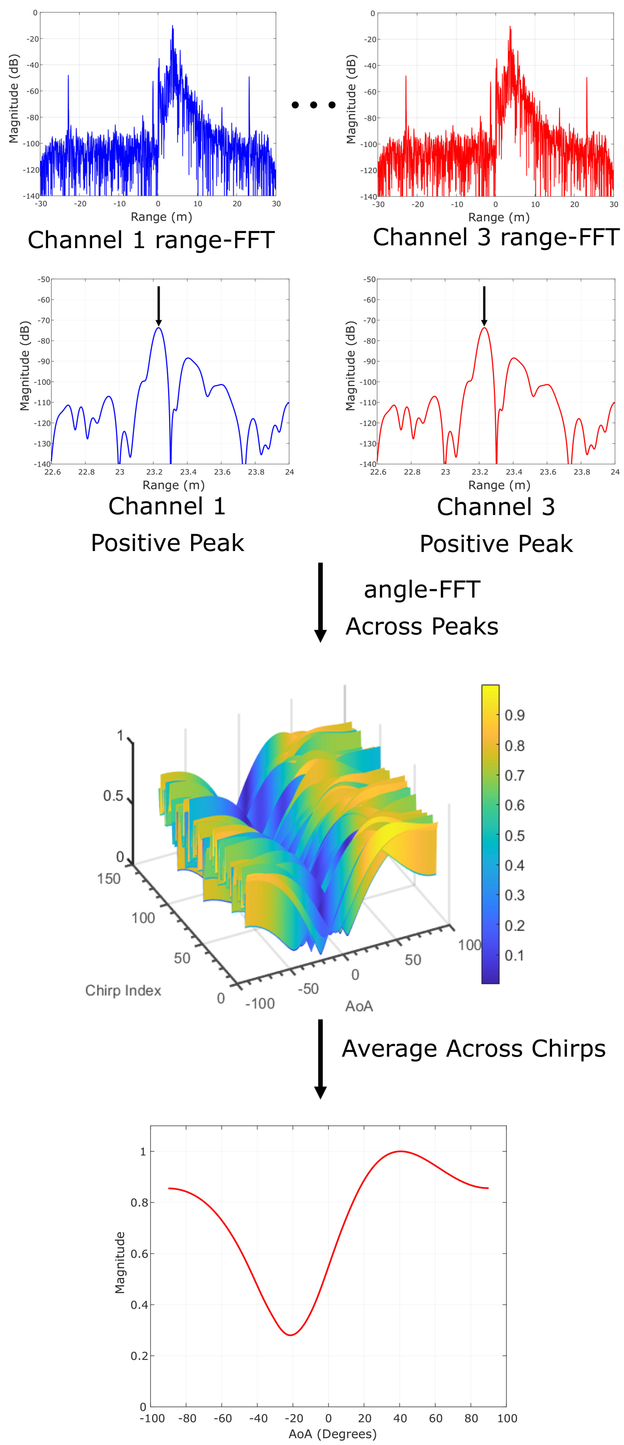

Fig. 9. Signal processing framework for AoA estimate with an AoA of 40 °.

1524 and the length of the range-FFT was 2^{17}, enabling zero-padding-based interpolation between the 1524 points in the range-FFT and an interpolated resolution of $0.228\,\mathrm{mm}$.

The range estimation of the tag for the subsequent results was calculated through the same process that has been described in the previous section. A range-FFT with a length of 2^{17} was taken along each chirp in the frame and the magnitude

TABLE III
CHIRP PARAMETERS USED TO ACQUIRE THE REPORTED MEASUREMENTS.

Parameter	**Value**
Bandwidth	$3.80\,\mathrm{GHz}$
Slope	$24.985\,\mathrm{MHz}/\mu\mathrm{s}$
Sampling Rate	$10\,\mathrm{MHz}$
Chirps per Frame	128
Chirp Periodicity	$160\,\mu\mathrm{s}$

spectrum of each range-FFT in the frame was then averaged. The two beat frequencies of the tag were found through a peak search algorithm after limiting the search to a window away from the modulating frequency which, for the case of these measurements, was a maximum distance of $50\,\mathrm{cm}$ away from the modulation frequency of the tag. Because the magnitude of the spectra of each chirps in a frame were averaged together to extract ranging information, each frame made up a single measurement. Based on the chirp periodicity, this constitutes an effective range-measurement rate of $20.48\,\mathrm{ms}$. The total of 128 frames were recorded for these measurements for each frame resulting in 128 range observations for each step in range away from the reader.

The after referencing the first range measure of $10\,\mathrm{cm}$ a constant offset was applied to the subsequent measurements. This allowed the calibration of the extra transmission line lengths present in the system. The results from the range measurements can be seen in Figure 10.

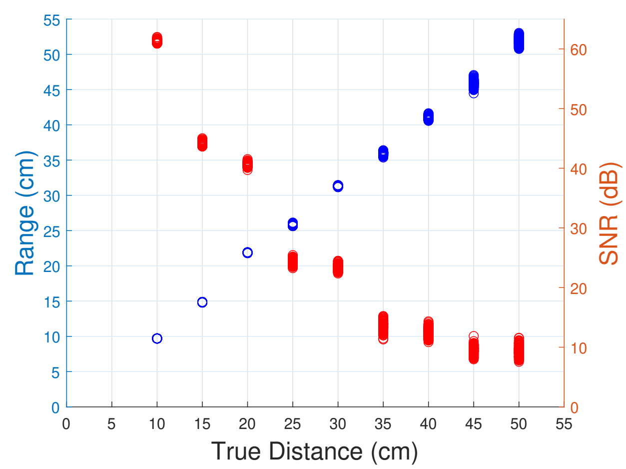

Fig. 10. Range estimate and SNR level of mmID tag positioned at boresight with respect to the reader.

The estimate of the range of the tag at boresight displays good agreement to the true range value—after applying the constant offset from the first range measurement—with a maximum standard deviation of $4.46\,\mathrm{cm}$ at $50\,\mathrm{cm}$. Also plotted in red is the signal-to-noise ratio (SNR) for each measurement at each range . Furthermore, the average error of the range estimate was calculated and a plot of the error over the measurement ranges is displayed in Figure 11. The range measurement displays a maximum error of $2\,\mathrm{cm}$, displaying the capability of the low cost mmID tag to be accurately located in a range of up to $0.5\,\mathrm{m}$ from the reader system. In comparison to UHF RFID localization systems, in [8], the authors present an UHF RFID system for localization that enables $4.03\,\mathrm{cm}$ accuracy of localization of a single RFID tag and reduces the median error to $2.76\,\mathrm{cm}$ for a localization utilizing three evenly spaced tags on an object. Additionally, the authors in [9] demonstrate a UHF RFID localization system with $11\,\mathrm{cm}$ median error. Therefore highlighting the ranging capabilities of the mmID system.

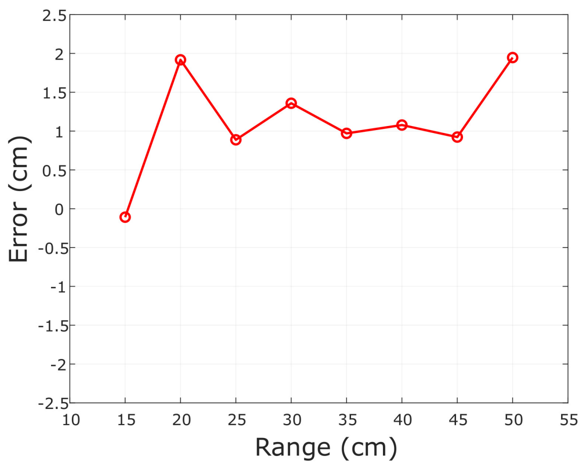

Fig. 11. Average error from the true value over the measurement range.

The Angle-of-Arrival results were taken with the mmID tag placed at a constant radial distance of $15\,\mathrm{cm}$ from the reader. Based on the antenna layout of the Antenna-on-Package (AOP) module, the receiving channels one and three were used for the azimuth AOA estimate of the tag. After processing the range-FFT along each chirp in each of the receiving channels and selecting the modulated beat frequency of the tag through a simple peak-select algorithm, an angle-FFT of length 2^{11} across this complex value was taken. After this process was complete, a magnitude average of the angular spectrum over all chirps in a frame was taken and, lastly, another peak-select algorithm was used for the AoA estimate. The mmID tag was moved from ± 40 with steps of 20. The results from the AoA measurements can be viewed in Table IV.

TABLE IV
AOA ESTIMATE MEASUREMENT RESULTS.

True AoA	Mean of Estimated AoA	STD of Estimated AoA
$-40\,^\circ$	$-38.91\,^\circ$	$1.19\,^\circ$
$-20\,^\circ$	$-21.74\,^\circ$	$0.65\,^\circ$
$0\,^\circ$	$0.65\,^\circ$	$0.58\,^\circ$
$20\,^\circ$	$21.79\,^\circ$	$0.83\,^\circ$
$40\,^\circ$	$39.82\,^\circ$	$1.52\,^\circ$

The maximum measured standard deviation from these AoA measurements was $1.52\,^\circ$ with a maximum average error of $1.74\,^\circ$. In comparison to UHF RFID localization systems, the authors in [10] demonstrated an AoA mean squared error of 2.39 over an angular coverage of ± 45. Additionally, the authors in [11] display a similar AoA error of 3.3. These results demonstrate the ability of the reader system to localize the tag angularly and with extremely high accuracy in a field of view of ± 40 in front of the reader with improved accuracy in comparison to UHF localization systems. The application of these processing methods to the entire MIMO system can extend the demonstrated 2D localization capability to 3 dimensions, as well as double its resolution.

V. Conclusion

The ultra-low cost, ultra compact mmWave mmID (mmID) system proposed in this work is a fraction of the cost of most commercially-available mmID systems. This is made possible through the benefits of operating within the $60\,\mathrm{GHz}$ ISM band and a small form-factor mmID and AOP radar system. This low-cost mmID presented has been localized in both range and angle with respect to the reader system. As displayed from the range measurements, the tag can be ranged at boresight at a distance of up to $0.50\,\mathrm{m}$ with a maximum standard deviation of $4.46\,\mathrm{cm}$ and an average accuracy of better than $2\,\mathrm{cm}$. Additionally, the system demonstrated great performance in estimating the AoA of backscattering signal, with an accuracy within $2\,^\circ$. Despite its currently unimpressive maximum range, a much greater potential lies beyond the capabilities demonstrated in this work. Indeed, as presented in [12] and [13], the range of the system has the potential to be greatly improved through the utilization of either a Rotman lens or Van-Atta structure instead of an individual patch antenna for the mmID tag. With the addition of cross-polarized TX and RX reader antennas, and further improvement in signal processing, the system could achieve maximum detection ranges in excess of 10x greater as estimated in Table II. This work potentially introduces a paradigm shift in the application of backscatter systems by introducing an affordable mmID-enabled real-time-microlocalization solution which could become ubiquitously installed in living environments and even worn for applications ranging from the smart home to automation, robotics, health monitoring, and Human Computer Interfaces.

References

[1] P. Pursula, T. Vaha-Heikkila, A. Muller, D. Neculoiu, G. Konstantinidis, A. Oja, and J. Tuovinen, "Millimeter-wave identification—a new short-range radio system for low-power high data-rate applications," *IEEE Transactions on Microwave Theory and Techniques*, vol. 56, no. 10, pp. 2221–2228, 2008.

[2] P. F. Freidl, M. E. Gadringer, D. Amschl, and W. Bcõsch, "mm-wave rfid for iot applications," in *2017 Integrated Nonlinear Microwave and Millimetre-wave Circuits Workshop (INMMiC)*, 2017, pp. 1–3.

[3] J. Kimionis, A. Georgiadis, and M. M. Tentzeris, "Millimeter-wave backscatter: A quantum leap for gigabit communication, rf sensing, and wearables," in *2017 IEEE MTT-S International Microwave Symposium (IMS)*, 2017, pp. 812–815.

[4] A. O. Adeyeye, J. Hester, and M. M. Tentzeris, "Miniaturized millimeter wave rfid tag for spatial identification and localization in internet of things applications," in *2019 49th European Microwave Conference (EuMC)*. IEEE, 2019, pp. 105–108.

[5] A. Strobel, C. Carlowitz, R. Wolf, F. Ellinger, and M. Vossiek, "A millimeter-wave low-power active backscatter tag for fmcw radar systems," *IEEE transactions on microwave theory and techniques*, vol. 61, no. 5, pp. 1964–1972, 2013.
[6] J. Lien, N. Gillian, M. E. Karagozler, P. Amihood, C. Schwesig, E. Olson, H. Raja, and I. Poupyrev, "Soli: Ubiquitous gesture sensing with millimeter wave radar," *ACM Transactions on Graphics (TOG)*, vol. 35, no. 4, pp. 1–19, 2016.
[7] W. Stein, A. Aleksieieva, S. Roehr, and M. Vossiek, "Phase modulated 61 ghz backscatter transponder for fmcw radar-based ranging," in *GeMiC 2014; German Microwave Conference*. VDE, 2014, pp. 1–4.
[8] J. Wang, F. Adib, R. Knepper, D. Katabi, and D. Rus, "Rf-compass: Robot object manipulation using rfids," in *Proceedings of the 19th Annual International Conference on Mobile Computing amp; Networking*, ser. MobiCom '13. New York, NY, USA: Association for Computing Machinery, 2013, p. 3–14. [Online]. Available: https://doi.org/10.1145/2500423.2500451
[9] J. Wang and D. Katabi, "Dude, where's my card? rfid positioning that works with multipath and non-line of sight," *SIGCOMM Comput. Commun. Rev.*, vol. 43, no. 4, p. 51–62, Aug. 2013. [Online]. Available: https://doi.org/10.1145/2534169.2486029
[10] S. Azzouzi, M. Cremer, U. Dettmar, R. Kronberger, and T. Knie, "New measurement results for the localization of uhf rfid transponders using an angle of arrival (aoa) approach," in *2011 IEEE International Conference on RFID*, 2011, pp. 91–97.
[11] C. Angerer, R. Langwieser, and M. Rupp, "Direction of arrival estimation by phased arrays in rfid," 01 2010.
[12] A. Eid, J. G. D. Hester, and M. M. Tentzeris, "Rotman lens-based wide angular coverage and high-gain semipassive architecture for ultralong range mm-wave rfids," *IEEE Antennas and Wireless Propagation Letters*, vol. 19, no. 11, pp. 1943–1947, 2020.
[13] J. G. D. Hester and M. M. Tentzeris, "A mm-wave ultra-long-range energy-autonomous printed rfid-enabled van-atta wireless sensor: At the crossroads of 5g and iot," in *2017 IEEE MTT-S International Microwave Symposium (IMS)*, 2017, pp. 1557–1560.